Journal of Neuroimmune Pharmacology (2025) 20:102
https://doi.org/10.1007/s11481-025-10257-8

RESEARCH

# Intravenous $^{64}$zn-Aspartate Mitigates Neuroinflammation and Motor Dysfunction in an Lps-Induced Parkinson's Disease Rat Model

Max Temnik[1] · Mariia Rudyk[2] · Alexandr Balakin[1] · Sergey Gurin[1] · Taisa Dovbynchuk[2] · Roman Byshovets[3] · Nataliia Dzubenko[4] · Ganna Tolstanova[4] · Larysa Skivka[2]

Received: 25 May 2025 / Accepted: 29 September 2025
© The Author(s) 2025

**Abstract**
Emerging evidence links zinc dyshomeostasis to the pathogenesis of Parkinson's disease (PD), highlighting the need to explore zinc-based interventions. Zinc has five stable isotopes, with $^{64}$Zn and $^{66}$Zn being the most abundant. Notably, healthy brain tissue is enriched in the lighter isotope $^{64}$Zn, while heavier isotopes are hypothesized to accumulate with age. This study examined the therapeutic potential of intravenously administered isotopically enriched $^{64}$Zn aspartate ($^{64}$Zn-asp) in a rat model of PD induced by a single stereotactic intranigral injection of lipopolysaccharide (LPS, 10 µg), which simulates acute neuroinflammation followed by progressive neurodegeneration. Treatment effects were evaluated using behavioral assessments, immunological profiling, biochemical and molecular analyses, and histopathology. Rats treated with $^{64}$Zn-asp showed a pronounced anti-inflammatory shift in microglial/macrophage metabolic profiles and reduced reactive astrogliosis. These changes were accompanied by improved motor performance and decreased anxiety-like behavior. Immunohistochemistry confirmed preservation of dopaminergic neurons. Overall, these findings suggest that $^{64}$Zn-asp attenuates neuroinflammation and supports neuronal survival, indicating its potential as a candidate for disease-modifying strategies in PD.

**Keywords** Parkinson's disease · Dopaminergic neurons · Stable light isotope enriched zinc aspartate · Neuroinflammation · Motor function · Anxiety-like behavior

## Introduction

Parkinson's disease (PD) is the second most commonly reported neurodegenerative disease after Alzheimer's disease. Currently, more than 10 million people worldwide are living with a PD diagnosis, ~90% of cases are considered sporadic (Willis et al. 2022; Safiri et al. 2023). Sporadic PD is a multifactorial neurologic disorder whose etiology and pathogenetic mechanisms remain unclear. Main pathological PD hallmark—movement disorder—is a result of the loss of dopaminergic neurons (DN) in the substantia nigra pars compacta. Key histopathological feature of PD are α-synuclein-containing Lewy bodies, which are commonly registered in areas of severe neuronal loss, and is a result of α-synuclein misfolding and aggregation into neurotoxic clumps. Oxidative stress associated with mitochondrial complex I dysfunction (Chen et al. 2019) and proteolytic stress due to dysfunction of the ubiquitin–proteasome system's autophagy pathway (Adam et al. 2023) are also considered important pathogenetic mechanisms of PD. More recently, chronic inflammation, both at the peripheral and cerebral levels, is considered an inevitable component of the pathological scenario in PD (Lee et al. 2019; Forloni et al. 2021). Despite considerable efforts, PD remains an incurable disease, for which treatment

✉ Mariia Rudyk
rudyk_marie@knu.ua

1 Physical Chemistry, North Miami Beach, Vector Vitale, Florida 33160, USA

2 Educational and Scientific Centre "Institute of Biology and Medicine", Taras Shevchenko National University of Kyiv, 2, Hlushkova Avenue, Kiev 03022, Ukraine

3 Department of Internal Diseases, Bogomolets National Medical University, 13, Shevchenko Blvd, Kiev 01004, Ukraine

4 Educational and Scientific Institute of High Technologies, Taras Shevchenko National University of Kyiv, 4G, Hlushkova Avenue, Kiev 03022, Ukraine

Published online: 12 November 2025

is limited to symptomatic therapy (Alfaidi et al. 2024; Berg et al. 2020). Numerous preparations with the potential to reduce neuroinflammation (non-steroidal anti-inflammatory drugs, microRNAs, leukotriene modifiers, Peroxisome Proliferator-Activated Receptor Gamma agonists, and many others) are widely examined in either animal/cell culture models of PD and in clinical trials, and are considered as a promising disease-modifying approach (Song et al. 2024; Çınar et al. 2022). Some of them are successfully used as an addition to conventional PD therapy (Khrieba et al. 2024). Common concerns associated with anti-inflammatory drugs are immunosuppressive effects, weakening the patrolling function of the immune system, and increased risk of infectious comorbidities (Hommel et al. 2022). The lack of effective pathogenetic therapies for PD underscores the need for continued research to uncover novel molecular mechanisms underlying its pathology and to identify new therapeutic targets. One of these mechanisms is zinc (Zn) dyshomeostasis (Park et al. 2014).

Zinc plays a crucial role in neurogenesis during both embryonic development and adulthood. Its dyshomeostasis is associated with impaired neuronal survival, migration, proliferation, and differentiation (Wang et al. 2023). Zinc also promotes proper protein folding and enhances the chaperone-like activity of human serum albumin, helping to prevent α-synuclein aggregation (Al-Harthi et al. 2022). Age-related zinc imbalance contributes to chronic meta-inflammation (inflammaging), a condition closely linked to increased risk of Parkinson's disease (de Oliveira et al. 2021). Zinc plays a vital role in neurogenesis during both embryonic development and adulthood. Its dyshomeostasis is linked to impaired neuronal survival, migration, proliferation, and differentiation (Wang et al. 2023). Disrupted zinc balance is closely associated with key mechanisms of Parkinson's disease (PD) pathogenesis since zinc supports proper protein folding, enhances the chaperone-like function of human serum albumin to prevent α-synuclein aggregation (Al-Harthi et al. 2022), maintains the ubiquitin–proteasome system (Reddy et al. 2022), and regulates cellular redox balance (Dabravolski et al. 2022). Age-related zinc imbalance contributes to chronic meta-inflammation (inflammaging), a known risk factor for PD (de Oliveira et al. 2021). Zinc also exhibits strong anti-inflammatory properties, primarily through modulation of NFκB signaling (Wessels et al. 2017). Importantly, it reduces inflammation without compromising immune surveillance by protecting cells from ROS-mediated damage and maintaining membrane integrity (Gammoh and Rink 2017).

Short-term oral zinc supplementation is considered a promising immune-enhancing strategy in geriatric care (Baarz et al. 2022). In animal models of neuropsychiatric disorders, zinc supplementation during pregnancy reduces neuroinflammation in offspring (Mousaviyan et al. 2021) and mitigates prenatal stress-induced behavioral and neurobiological impairments in adolescent female rats (Sameei et al. 2023). Moreover, zinc improves lifespan and motor function in *Drosophila* with mutant Parkin (Saini and Schaffner 2010), and shows neuroprotective effects in rotenone-induced PD in rats by reducing lipid peroxidation and neuronal death (Mbiydzenyuy et al. 2018).

All previous studies have used zinc compounds with natural isotopic composition. Zinc has five stable isotopes – $^{64}$Zn, $^{66}$Zn, $^{67}$Zn, $^{68}$Zn, and $^{70}$Zn – with natural abundances of 48.6%, 27.9%, 4.1%, 18.8%, and 0.6%, respectively. The most abundant, $^{64}$Zn and $^{66}$Zn, form the basis for measuring zinc isotopic composition in tissues, typically expressed as $\delta^{66}$Zn (Jaouen et al. 2019). In a healthy brain, the lighter isotope $^{64}$Zn predominates ($\delta^{66}Zn < 1$), due to differential bonding: heavier isotopes bind more strongly to oxygen- and nitrogen-containing ligands (e.g., phosphate, lactate, histidine), while lighter isotopes prefer sulfur-containing ligands like cysteine and methionine. Most brain zinc is bound to cysteine residues in metallothioneins (Tanaka and Hirata 2018; Solovyev et al. 2021).

Current hypotheses suggest that heavier zinc isotopes accumulate with age, increasing $\delta^{66}$Zn in tissues (Albarede et al. 2016; Jaouen et al. 2019). This shift is especially pronounced in neurodegenerative disorders involving protein misfolding (Moynier et al. 2020). For example, in Alzheimer's disease, heavy zinc isotopes preferentially bind histidine residues in the N-terminal region of amyloid-β (Aβ), particularly in plaques. Though metal binding in α-synuclein remains underexplored, histidine at residue 50 – a key binding site for heavy zinc (Ramis et al. 2018) – is critical for its misfolding and aggregation into neurotoxic clumps (Brown 2009; Nakamura et al. 2023).

Zinc supplements are typically administered orally, but their therapeutic effectiveness is often limited, possibly due to an age-related decline in intestinal zinc absorption. Parenteral supplementation offers a potential solution to this issue (Cvijanovich et al. 2016; Baltaci et al. 2024; Gumus et al. 2023). To our knowledge, this is the first study to investigate the effects of intravenous (i.v.) delivery of isotopically modified zinc in an animal model of PD. The aim was to assess the impact of i.v. administration of $^{64}$Zn aspartate ($^{64}$Zn-asp) on neuroinflammation and related motor dysfunction in rats with LPS-induced (inflammatory) PD model.

We used a novel $^{64}$Zn-asp enriched with the light isotope $^{64}$Zn to 99.2%—a substantial increase from the natural abundance of 48.6% typically found in zinc supplements. Previous studies showed that $^{64}$Zn-asp has greater biological activity than zinc aspartate with a natural isotopic composition (Novak et al. 2022a; Novak et al. 2022b).

## Materials and Methods

### Test Agent

Isotopically modified $^{64}$Zn di-aspartate ($^{64}$Zn-asp, KLS-1), an investigational new complex of zinc aspartate (Fig. 1), was used as a therapeutic test agent. The compound molecule consists of two molecules of L-aspartic acid (Neo-Froxx, Einhausen, Germany) and one atom of $^{64}$Zn, having its molecular formula of $C_8H_{12}O_8N_2{}^{64}Zn$ (Fig. 1).

The molar mass of the compound in solution is 328 g/mol. The proportion of zinc in the compound is 17.98%. The zinc in the compound consisted of stable light isotope $^{64}$Zn enriched to 99.2% mass fraction of total zinc. KLS-1 was manufactured by Pharmaceutical Factory Biopharma LLC (Bila Tserkva, Ukraine)—forming a chelate complex.




**Fig. 1** Schematic representation of the investigational new compound structure

### Animals, Study Design, and LPS-PD Model

**Animals** Experiments were conducted on adult male Wistar rats (8 weeks old, 220–250 g) bred in the vivarium of the Educational and Scientific Centre "Institute of Biology and Medicine" of Taras Shevchenko National University of Kyiv, Ukraine. The animals were kept in standard conditions with ad libitum access to water and food (standard diet). Animal protocols were approved by the University Ethics Committee (protocol No 4, 10.10.2021) according to Animal Welfare Act guidelines. All procedures with animals were performed in accordance with the principles of humanity as stated in "General principles of animal experimentation" approved by the National Congress on bioethics (Kyiv, 2001–2007) and in concordance with Council directive of November 24, 1986 on the approximation of laws, regulations and administrative provisions of the Member States regarding the protection of animals used for experimental and other scientific purposes (86/609/EEC).

**Study Design and LPS-PD Model** Before the experiment, 66 adult male Wistar rats were randomly divided into 4 groups using the "RAND ()" function in Microsoft Excel (Fig. 2A): group I—intact animals (n = 12); group II—sham-operated animals (n = 12); group III—LPS-PD (n = 12); group IV – rats with LPS-PD treated with $^{64}$Zn-asp (n = 15). In order to attain unilateral lesions of the nigrostriatal system in animals from group III and IV, stereotaxic microinjections of 10 µg of LPS (Lipopolysaccharide from Escherichia coli O111:B4, Sigma) at a volume of 2 µl of sterile physiological saline (JSC "Infusion", Ukraine) were conducted. Animals from group II were injected with 2.0 µL of sterile physiological saline. Before the surgery, rats from groups II-IV were anesthetized with a mixture of ketamine (75 mg/kg diluted in sterile water for injection, Sigma, USA)

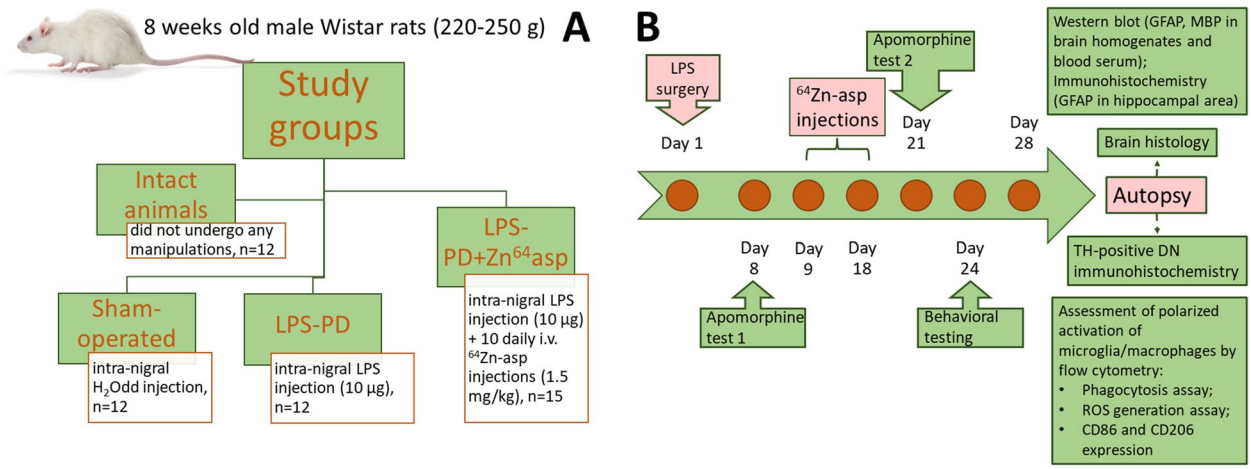


**Fig. 2** Animal groups (A) and study design (B)

and 2% Xylazine (400 µl/kg, Alfasan International BV, Netherlands) i.p, placed in a stereotaxic instrument (SEJ-4, Ukraine). After that, either LPS or sterile physiological saline was injected unilaterally into the brain through the drilled burr hole directly into the substantia nigra (AP 5.3 mm, ML±2.0 mm (from bregma), and DV 7.2 mm (below dura)) according to Hoban et al. (2013). The injections were performed at a rate of 1 µl/min (every 15 s). The injector was left in place for 5 min before slowly withdrawing it to allow for the toxin diffusion and to prevent the toxin reflux. The period of 8 days was allowed for the development of the LPS-induced model of Parkinson's disease (PD). Animals from group IV received 10 daily i.v. injections of $^{64}$Zn-asp into the lateral tail vein at a dose of 1.5 mg/kg starting from Day 9 after the disease initiation. PD development was ascertained by the results of behavioral testing, post-mortem histological examination of the rat brains, and assessment of nigrostriatal neurodegeneration using semi-quantitative tyrosine hydroxylase (TH) immunohistochemistry. Metabolic profile of microglia/macrophage population, as well as astroglia assessment, was evaluated at the time point of the experiment cessation (Day 28 after the surgery) (Fig. 2B).

## Behavioral Testing

**Open Field Test** An open field test was conducted on Day 24 after the surgery as described by Leite-Almeida et al. (2009). To evaluate voluntary movement, anxiety, and exploratory behavior in a new environment, the rats were tested in the Open Field arena, which consisted of a square field with sides of 100 cm and a wall height of 30 cm, illuminated by two LED lamps (each with 60 W) placed at a height of 2 m, for 5 min. A grid of 36 squares was drawn on the bottom of the arena. During testing, each animal was individually placed in the center of the arena and its ambulatory activity was recorded using a digital camera ("Casio® EX-Z850", China, which was located above the center of the arena at a height of 1 m), followed by the analysis using MATLAB. The following behavioral characteristics were assessed: total distance travelled, time spent exploring the inner perimeter, time spent in squares surrounded by two walls (thigmotaxis), number of rearing and grooming, frequency of defecations (Sestakova et al. 2013; Lamprea et al. 2008). The arena was cleansed and allowed to dry after each animal test.

**Apomorphine-Induced Rotation Test** The apomorphine test was conducted on Day 8 and Day 21 after the surgery. Apomorphine (A4393, Sigma, USA) was i.p. administered to the lesioned rats at a dose of 0.5 mg/kg (Ferreira et al. 2020; Talanov et al. 2006). Five minutes after the injection, the rats were put individually into a 40 cm-diameter cylinder, and the counterclockwise (contralateral) rotations were monitored and registered for 30 min using a stopwatch. Animals scoring over 6 rpm were considered as lesioned with 86.6% DN loss. Rats scoring less than 6 rpm (0–2 rpm) were considered as lesioned with 44% DN loss (Talanov et al. 2006).

**Elevated Plus Maze (EPM) Test** EPM test was used to assess anxiety-like animal behavior and was conducted on Day 24 after the surgery (Walf and Frye 2007). EPM raised to a height of 50 cm from the floor consisted of a cross-shaped field with two opposite open arms (50 cm × 10 cm) and two closed arms (50 cm × 10 cm × 30 cm). These four arms were connected to a center square with sides 10 cm into which, facing the open sleeve, the animal is placed at the beginning of the test. The setup was illuminated by two LED lamps, each 60 W, which are located at a height of 2 m. The experiment is recorded on an IP camera, after which the parameters are evaluated using MATLAB. Behavioral assessment was performed using the following main parameters: total distance traveled, number of transitions from open to closed arms, number of transitions from closed to open arms, time spent in open and closed arms, total number of transitions, and time spent in a stretched attend posture (risk assessment) (Walf and Frye 2007). The testing was conducted for five minutes. Before starting the measurements, animals underwent an adaptation period to the new environment in order to reduce their stress state.

## Histological Examination of the Rat Brains

A procedure of rapid, controlled, and uniform fixation of the entire body of the animal was carried out under light ether anesthesia using 4% buffered paraformaldehyde (Diapath, Italy) perfused through the rat's heart (Gage et al. 2012). The brain was carefully removed and fixed in 10% neutral formalin (Diapath, Italy). Fixed frontal tissues were dehydrated and embedded in Paraplast (Surgipath Paraplast, Leica, USA). 6-µm-thick paraffin sections of the brain were cut using a Thermo Microm HM 360 microtome (Thermo Scientific, USA). Sequentially, the sections were deparaffinized, rehydrated, and stained with hematoxylin and eosin (Thermo Scientific, USA) using standard procedures (Falkeholm et al. 2001; Buesa and Peshkov 2011). The topography of the substantia nigra of the rat midbrain was determined using a stereotaxic atlas (Paxinos and Watson 1982). The presence of a microinjector track served as a criterion for the localization of the damage zone in brain samples from rats of experimental groups (groups II-IV). The

stained slides were examined using an Olympus BX51 microscope (Olympus, USA). Microphotographs of homotopic areas of the substantia nigra were obtained, and morphometric analysis of changes in the average cross-sectional areas of neuron bodies (perikaryons) was performed using AxioVision SE64 Rel. 4.9.1 software (Carl Zeiss, Germany) at a magnification of × 400.

## Immunohistochemistry

For immunohistochemical staining of rat brain sections with antibodies to tyrosine hydroxylase (TH), rats were deeply anesthetized and transcardially perfused with heparinized (5000 U/L) sterile physiological saline (100 mL) followed by 4% paraformaldehyde (150 mL, pH 7.4). The brains were removed, post-fixed in 4% paraformaldehyde, and sectioned. The paraffin-embedded Sects. (5 µm) were processed for TH immunohistochemical detection using the ABC-peroxidase method as described previously (Walsh et al. 2011). Briefly, tissue sections were first incubated with tyrosine hydroxylase (TH) primary antibodies (1:200, Millipore, AB152, USA) overnight (4 ºC), and then with the secondary anti-rabbit biotinylated antibodies (1:200) for 60 min. After this, Diaminobenzidine (Dako, EnVision Flex, DM821, USA) immunoreactivity detection system was applied for 5 min. Stained sections were assessed using a Primo Star microscope (Carl Zeiss, Germany). Each sample was scored semi-quantitatively as to the intensity of immunostaining on a four-point scale, with 0 indicating absence of staining (< 10% of positive cells), 1 + indicating the lowest level of detectable staining (10–25% of positive cells), 2 + indicating moderate homogeneous staining (25–50% of positive cells), 3 + indicating intense homogeneous staining (50–75% of positive cells), and 4 + (> 75% of positive cells) (Pauletti et al. 2000). The results were scored by multiplying the percentage of positive cells (P) by the intensity (I) and presented as the Quick score (Q): Q = P x I.

Hippocampal sections were prepared to detect GFAP expression in the rat brain tissue using confocal microscopy. The sections were blocked with 3% bovine serum albumin (Sigma-Aldrich, Germany) for 60 min at room temperature. The tissue sections were incubated with primary anti-GFAP antibodies (Santa Cruz Biotechnology, USA) at + 4˚C overnight. Sequentially, the samples were incubated for 60 min at room temperature with FITC-conjugated secondary antibodies (Santa Cruz Biotechnology, USA) diluted 1:500. The slides were rinsed and stained with fluorescent dye Hoechst-33342 (Invitrogen, United Kingdom) to visualize the cell nucleus. Immunofluorescence results were analyzed using an LSM 510 META microscope (Carl Zeiss, Germany) and processed using ImageJ software (Fiji, USA).

## Western Blot Analysis

To isolate proteins, freshly isolated rat brain samples were rapidly placed in liquid nitrogen and crushed. Sequentially, the brain tissues were lysed and proteins were extracted using RIPA buffer (Sigma-Aldrich, USA). All lysates were subsequently sonicated three times for 30 s (Sartorius, Labsonic® M, Canada) and centrifuged at 16000 g for 30 min at + 4 °C (Sigma-Aldrich, USA). The protein concentrations in rat brain samples were measured using the Modified Lowry Protein Assay Kit (Thermo Scientific, USA) following the manufacturer's instructions. Supernatants were diluted with 5 × Laemmli sample buffer (Sigma-Aldrich, USA) containing 0.1 M dithiothreitol (Sigma, USA) and boiled for 5 min. Protein samples were subsequently frozen and stored at −20 °C. Protein electrophoresis was performed in Tris–glycine buffer (pH 8.3) (Sigma-Aldrich, USA) using a Mini-PROTEAN II electrophoresis chamber (BIO-RAD, USA) at a voltage of 100 V for 90 min. To determine molecular weights of proteins on electropherograms, protein standards covering a molecular weight range of 10–250 kDa (Thermo Scientific, USA) were used. Proteins were transferred from polyacrylamide gel (Sigma-Aldrich, USA) onto a 0.45-µm poresize nitrocellulose membrane (RPN203D, GE Healthcare, Amersham Bioscience) using the Mini Trans-Blot Cell (BIO-RAD, USA) in a transfer buffer containing 2.5 mmol/L Tris–HCl, pH 8.3, 20% methanol, 192 mmol/L glycine, 0.1% SDS (Sigma-Aldrich, USA). Free binding sites on the membrane were blocked with 5% skim milk (Genesee Scientific Inc., USA). The membrane was incubated with primary anti-GFAP antibodies (Santa Cruz Biotechnology, USA), myelin basic protein (MBP) (Santa Cruz Biotechnology, USA) or beta-actin (Santa Cruz Biotechnology, USA) diluted in phosphate buffer saline containing 0.05% Triton X-100 (Sigma-Aldrich, USA) following the manufacturer's instructions at + 4˚C overnight. Sequentially, the membrane was incubated with horseradish peroxidase-conjugated secondary antibodies (Santa Cruz Biotechnology, USA) for 60 min. Immunoreactive bands were visualized using enhanced chemiluminescence. Densitometric analysis of autoradiograms was performed using TotalLab TL120 software (Nonlinear Inc., USA), and the intensity of bands was normalized to the intensities of corresponding beta-actin bands. The protein number was reported in arbitrary units (a.u.).

## Microglia/macrophage cell isolation

For microglia/macrophage cells isolation, the brain was rapidly extracted on ice. Hippocampus was dissected and perfused using a phosphate-buffered saline (PBS). Isolated tissue was softly dissociated in ice-cold PBS supplemented with 0.2% glucose for 15 min at room temperature using

a Potter homogenizer. Tissue homogenate was filtered through a 40 nm cell strainer (BD Biosciences Discovery) for additional tissue grinding and subsequently transferred to a 15 mL tube and centrifuged at 350 g for 10 min at room temperature. Cell sediment was suspended in 1 ml of 70% isotonic Percoll solution. 1 ml of 50% Percoll solution was gently layered on top of the 70% layer, and 1 ml of PBS solution was subsequently layered on top of the 50% Percoll layer. The density gradient was centrifuged for 40 min at 1200 g. After centrifugation, the layer at the interface between the 70% and 50% Percoll phases, which contained highly enriched microglia/macrophage, was aspirated, and the cells were washed twice in PBS by centrifugation (Frank et al. 2006). Purity of isolated microglia/macrophage fraction was examined by flow cytometry using fluorescein isothiocyanate (FITC) mouse anti-rat CD11b (BD PharmingenTM) and phycoerythrin (PE) mouse anti-rat CD45 (BD PharmingenTM). The proportion of CD11b+CD45+cells was 88.9±3.7%. Cell viability was determined by the Trypan blue exclusion test. The proportion of viable cells was ≥93%.

### Phagocyte metabolic profile assessment

A phagocyte metabolic profile was characterized by their phagocytic activity, oxidative metabolism, and phenotypic marker expression, which were examined by flow cytometry. Phagocytic activity was detected as described earlier (Rudyk et al. 2018). FITC-labeled thermally inactivated cells of Staphylococcus aureus Cowan I (collection of the Department of Microbiology and Immunology, ESC "Institute of Biology and Medicine" of Taras Shevchenko National University of Kyiv) were used as a phagocytosis object. $2 \times 10^5$ microglia/macrophage cells were incubated at 37 °C for 30 min with bacterial cells (5 µL of the stock suspension of FITC–labeled S. aureus at a concentration of $1 \times 10^7$ cells/mL). Phagocytosis was stopped by adding a 'stop' solution (PBS with 0.02% EDTA and 0.04% paraformaldehyde). The data was presented as the phagocytosis index (PhI) representing the mean fluorescence per one phagocytic cell (ingested bacteria by one cell), and as phagocytosis percentage (PP) (percentage of cells emitting fluorescence). The phagocyte oxidative metabolism was examined using 2′7′-dichlorodihydrofluorescein diacetate (H2DCFDA, Invitrogen) as described previously (Rudyk et al. 2018).

For phagocyte phenotyping, FITC-labeled anti-CD86, PE-labeled anti-CD80, and Alexa Fluor 647-labeled anti-CD206 antibodies (BD Pharmingen, USA) were used. Results were assessed using a FACSCalibur flow cytometer and CellQuest software (BD, USA).

### Statistical analysis

Statistical analysis was conducted using the Statistica 12.0 package. First, the data were tested for normal distribution using the Shapiro–Wilk test (Mishra et al. 2019). Normally distributed variables were presented as mean±SD. Non-normally distributed variables were presented as the median and interquartile range (IQR). Statistical differences were calculated using ANOVA with Tukey's post-hoc test for multiple comparisons of variables with a normal distribution, and non-parametric Mann–Whitney U test for single comparisons, and Kruskal–Wallis's test for multiple comparisons of variables with a non-normal distribution (Chan and Walmsley 1997). Differences were considered significant at $p \leq 0.05$.

## Results

**Treatment with $^{64}$Zn-asp mitigated reactive astrogliosis in rats with LPS-PD.** Reactive astrogliosis is a common pathological hallmark of neurodegeneration and a key component of neuroinflammation (Kwon and Koh 2020). Reactive astrogliosis is accompanied by enhanced fibrillogenesis due to increased expression of glial fibrillary acidic protein (GFAP), the main intermediate filament protein component of the astrocyte cytoskeleton (Liddelow et al. 2017). Soluble GFAP breakdown products, which are released into interstitial fluid and are also found in serum, indicate neuroinflammation and neurodegeneration (Yamashita et al. 2023). In our experiments, GFAP levels in brain homogenates of LPS-lesioned rats were ~2 times higher than those of rats from control groups (Fig. 3A, B). Results of Western blot analysis were confirmed by immunohistochemistry assay of hippocampal sections. Strongly increased immunoreactivity for GFAP was observed in LPS-lesioned rats (Fig. 3D). Treatment with $^{64}$Zn-asp was associated with a decrease in GFAP-immunoreactive areas in the hippocampus of the rats with LPS-PD. The content of GFAP breakdown products in brain homogenates of rats from the LPS-PD group was about 2.5 times higher than that in intact animals, and more than 6 times higher than compared in sham-operated rats (Fig. 3C). Slightly elevated content of GFAP and its breakdown products was also registered in serum, further indicating reactive astrogliosis in LPS-PD rats (Fig. 3F, G). After treatment with $^{64}$Zn-asp (LPS-PD+$^{64}$Zn-asp group), the content of GFAP and its breakdown products in animal brain homogenates decreased almost to the level of control animals. $^{64}$Zn-asp injections in LPS-lesioned rats resulted also in a significant decrease of serum levels of GFAP and its breakdown products, additionally indicating that reactive astrogliosis is mitigated.

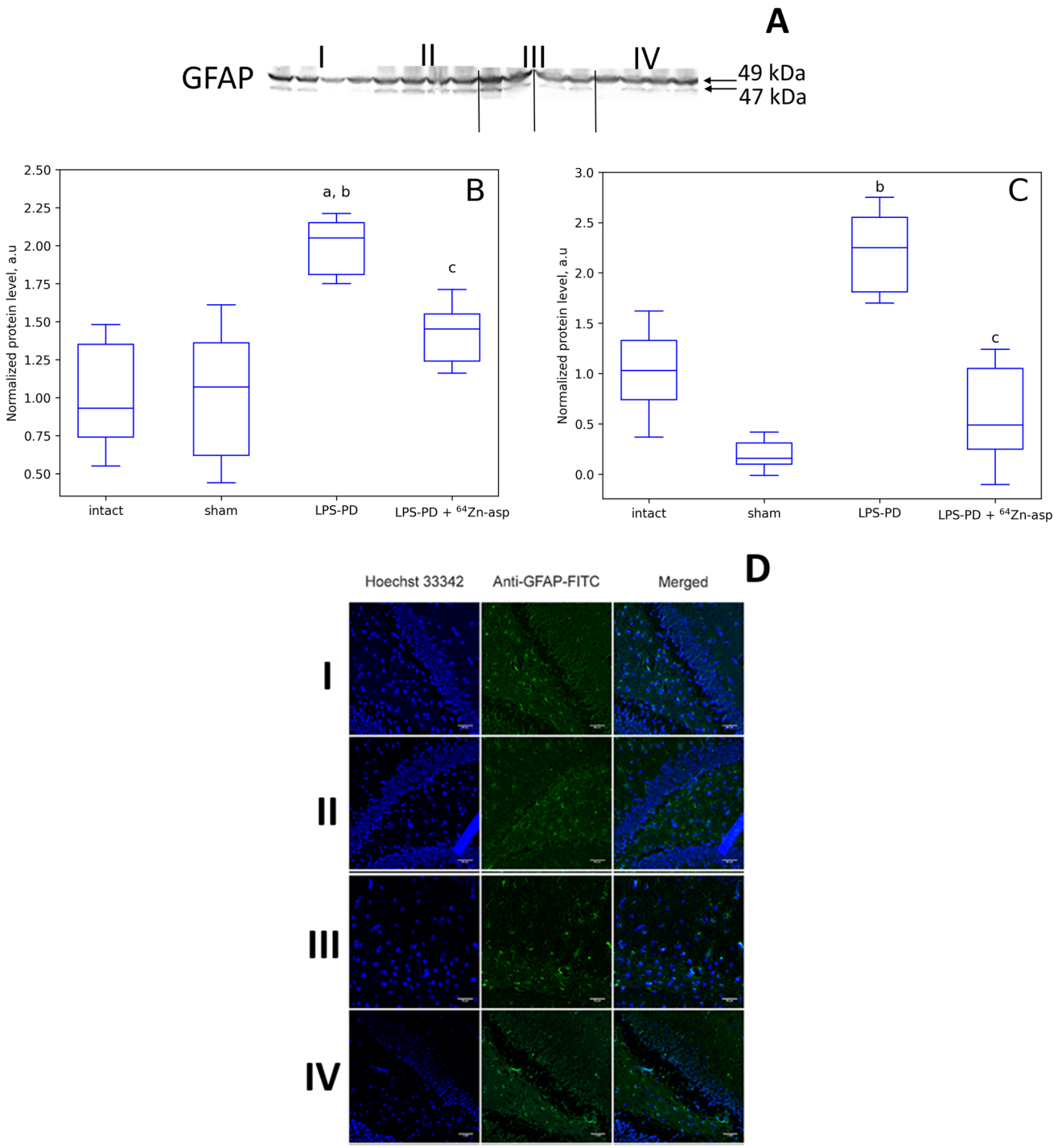


**Fig. 3** Effect of treatment with $^{64}$Zn-asp on astroglia in LPS-lesioned rats. Western blot analysis (A) and results of blotogram densitometry of total GFAP pool (B), GFAP breakdown products (C), and MBP (E) in rat brain homogenates. D—representative immunohistochemical images of the GFAP-positive neurons in hippocampal area: I—intact animals, II—sham-operated animals, III—LPS-PD, IV—LPS-PD+$^{64}$Zn-asp. Sections were treated with antibodies against GFAP, and nuclei were stained with Hoechst-33342, confocal microscopy (scale bar—50 μm). Results of blotogram densitometry of total GFAP pool (F) and GFAP breakdown products (G) in rat blood serum. Numerical data are presented as medians and IQR. a—$p \leq 0.05$ as compared to intact animals, b—$p \leq 0.05$ as compared to sham-operated animals; c—$p \leq 0.05$ as compared to LPS-PD group (Kruskal–Wallis's test). Note: Western blot images were cropped, and lanes were spliced for clarity. Splicing sites are indicated by vertical lines. No other modifications were applied, and all samples were run on the same gel

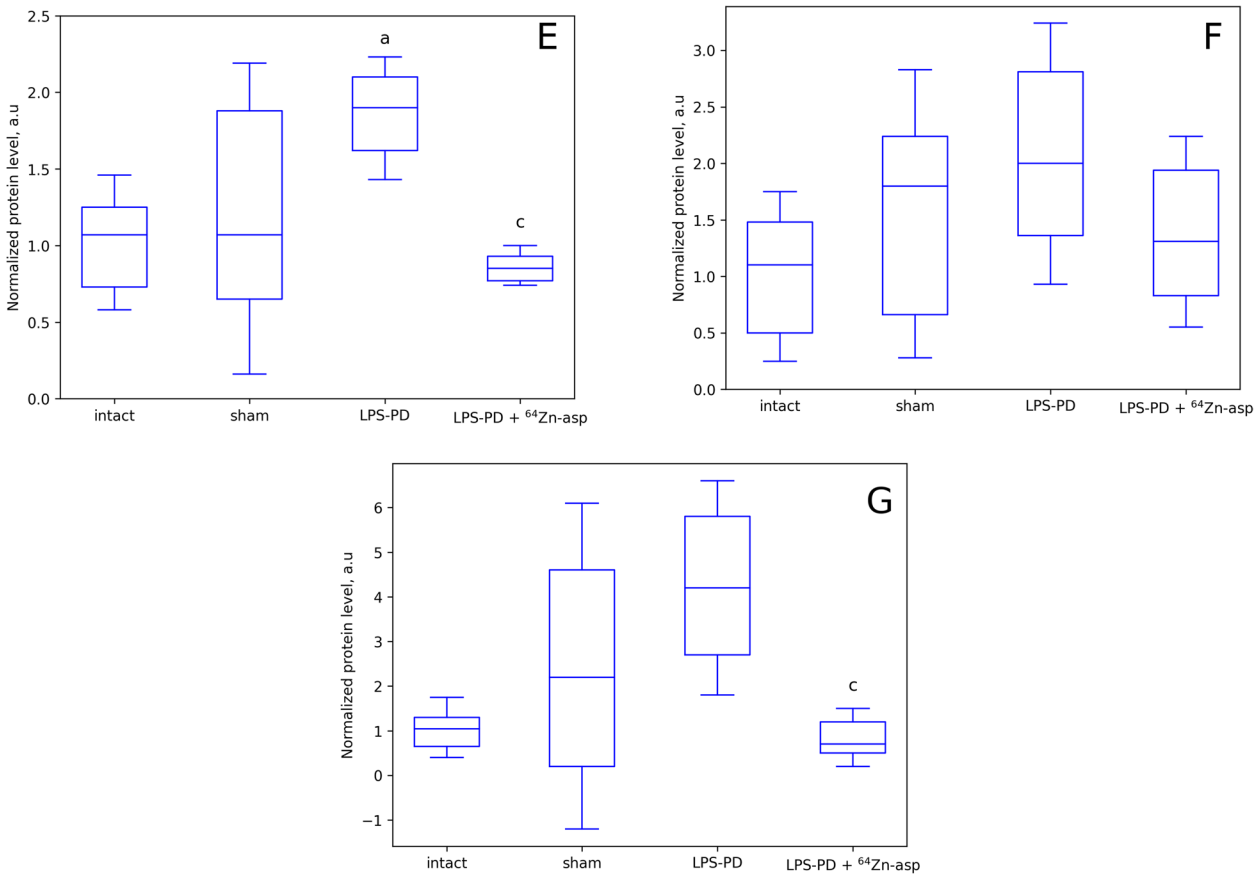


**Fig. 3** (continued)

Reactive astrocytes can negatively affect myelination/remyelination and can even cause demyelination (Nash et al. 2011). In our experiments, we used Western blot for assessing MBP content in rat brain homogenates. The rat brain MBP is represented by two forms: high molecular weight polypeptides (95–110 kDa), which are components of Schwann cell membranes, and a monomeric, relatively low molecular weight form (17 kDa), which is predominantly cytosolic. Assessing MBP content and its polypeptide composition in brain tissue is used to characterize the degree of neuron demyelination/remyelination (Weil et al. 2016). In our experiments, the level of high molecular weight MBP polypeptides (95–110 kDa) in the brain homogenates of animals with LPS-PD was 1.8 times higher than compared of control animals (Fig. 3E). In rats with LPS-PD given the $^{64}$Zn-asp injections, a decrease in the level of MBP was observed almost to the control values.

**Treatment with $^{64}$Zn-asp shifted the metabolic profile of the microglia/macrophage population in rats with LPS-PD** In our experiments, a complex population of microglial (MG) cells was examined. In the healthy brain of intact animals, yolk sac-derived resident microglial cells predominate with a minor fraction of border-associated macrophages (BAM), whereas in lesioned animals, the macrophage fraction is larger due to blood monocytes recruited in the course of neuroinflammation (Silvin et al. 2023). Since counteracting NF-κB signaling is one of the key mechanisms of zinc anti-inflammatory effects, in our experiments, the metabolic profile of the complex MG population was characterized by assessing principal NF-κB-dependent phagocyte functions: phagocytic activity, ROS generation, and expression of phenotypic markers CD86 and CD206. Phagocytic activity was assessed using bacterial cells as phagocytosis objects. Bacterial phagocytosis is a toll-like receptor (TLR)-dependent process, and S. aureus phagocytosis involves NF-κB activation (Zhu et al. 2014). Intracellular ROS generation involves transcription of NF-κB-dependent genes, although the levels of NF-κB activity are also regulated by the levels of ROS generation. Antigen-presenting capacity (including MHC- and co-stimulatory molecules CD80/86 expression) is dependent on NF-κB activation (Mussbacher et al. 2023). NF-κB also governs mannose receptor functioning, and NF-κB inhibitors reduce the CD206 expression (Cornice et al. 2024). In our experiments, different patterns of MG metabolic state were observed in different animal groups. Metabolic characteristics

of the MG population in sham-operated animals indicated an activated state of these cells with a slight skew to M2b (anti-inflammatory, immunoregulatory) phenotype: increased fraction of phagocytizing cells and elevated phagocytic activity (Fig. 4A, B), augmented ROS generation (Fig. 4C), but decreased CD206+cell fraction (Fig. 4E) (Kisucká et al. 2021; Wang et al. 2023) as compared to intact animals. This may be due to the resolution of neuroinflammation, which is characteristic after surgical trauma during the placebo surgery (Alam et al. 2018). Values of PP, PI (Fig. 4A, B), and ROS

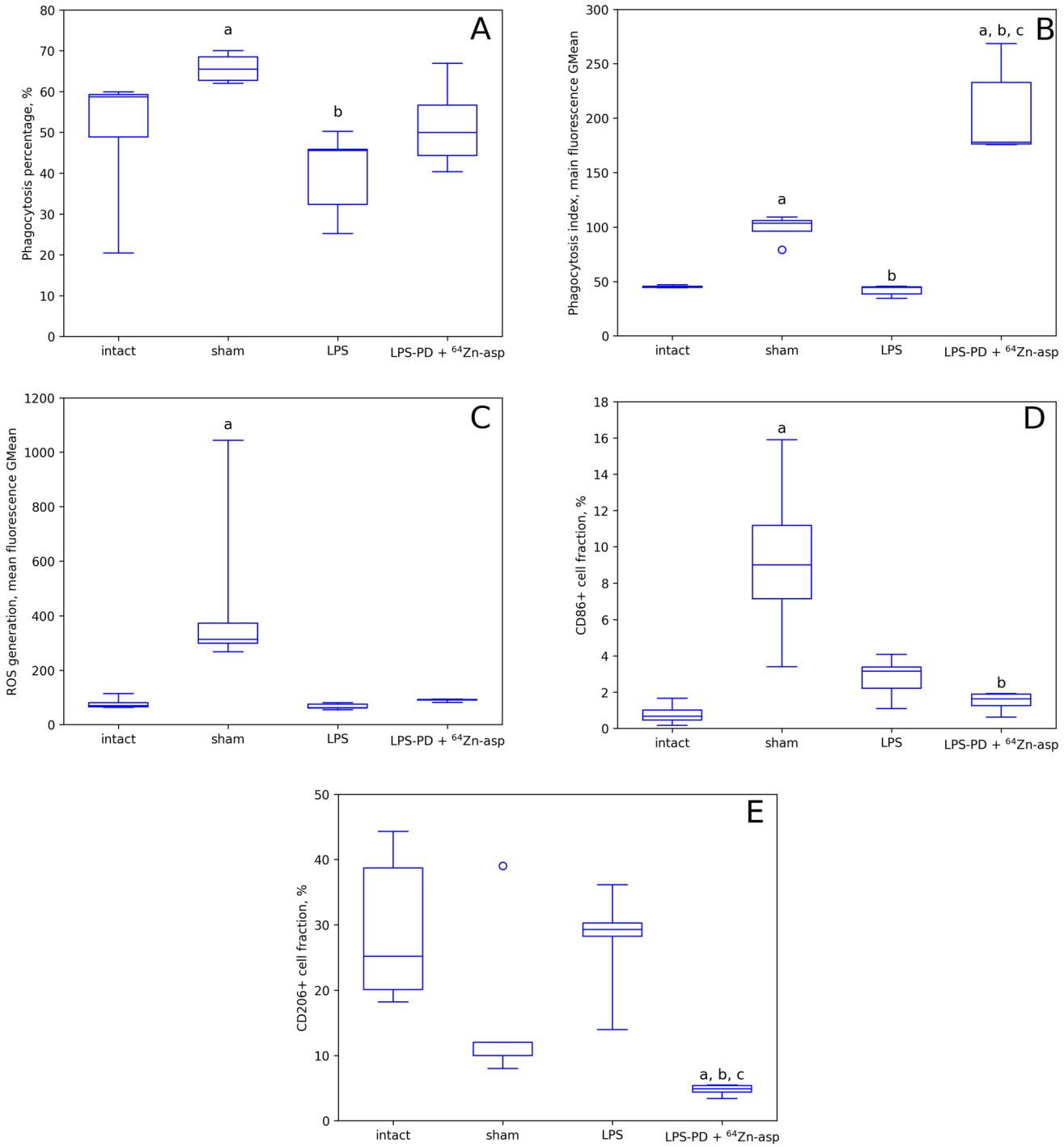


**Fig. 4** Effect of treatment with.$^{64}$Zn-asp on metabolic characteristics of microglia/macrophages in LPS-lesioned rats. A – phagocytosis percentage; B – phagocytosis index; C – ROS generation; D – fraction of CD86-positive cells; E – fraction of CD206-positive cells. Data are presented as medians and IQR. a—$p \leq 0.05$ as compared to intact animals, b—$p \leq 0.05$ as compared to sham-operated animals; c—$p \leq 0.05$ as compared to LPS-PD group (Kruskal–Wallis's test)

generation (Fig. 4C) in MG of rats from the LPS-PD group did not differ significantly from those in intact animals, and were lower than those in sham-operated rats. CD86+cell fraction in these animals was slightly smaller than that in sham group and somewhat enlarged as compared to that in intact rats (Fig. 4D). CD206+cell fraction in LPS-PD animals did not differ from that in intact rats and was higher than in animals from sham group (Fig. 4E). Given the presence of neuroinflammation, which was evidenced by reactive astrogliosis, functional profile of MG in LPS-PD rats can be characterized as metabolic exhaustion with a residual level of pro-inflammatory polarized activation (Pérez and Rius-Pérez 2022; Yunna et al. 2020). Treatment of LPS-lesioned rats with $^{64}$Zn-asp significantly increased the phagocytic activity of microglia, slightly reduced the CD86+cell fraction, and markedly decreased the proportion of CD206+cells.

The fact, that PI median values in the LPS-lesioned rats treated with $^{64}$Zn-asp were the highest and had surpassed similar indicators in the intact animals, the sham-operated and the LPS-lesioned untreated animals by 3.9, 1.7 and 4 times correspondingly indicates potent stimulatory effects of $^{64}$Zn-asp on the phagocytic (scavenging) capacity of microglia/macrophage cells, that is characteristic for the M2a (tissue healing, neuroprotective) MG phenotype (Wang et al. 2023).

**Treatment with $^{64}$Zn-asp prevents body weight loss in LPS-lesioned rats.** Body weight loss is typical for patients with PD. This can be caused by decreased food intake, elevated energy expenditure, or gastrointestinal dysfunction, and is associated with poor prognosis (Cumming et al. 2017). At the time of experiment cessation (Day 28), the weight of intact animals increased by 36% as compared to initial values (Fig. 5A). Sham-operated rats gained their weight by 30,6% over this time period, whereas the body weight of LPS-lesioned animals did not change for the whole of the study's observation time. LPS-lesioned rats, which received $^{64}$Zn-asp injections, demonstrated a slight increase in weight (by 12%) at this time point. It is necessary to note that initial body weight values in LPS-PD and LPS-PD+$^{64}$Zn-asp did not differ significantly (Fig. 5B).

**Treatment with $^{64}$Zn-asp reduced DN loss and behavioral alterations in rats with LPS-PD** Inhibition of neuroinflammation in LPS-lesioned rats after the treatment with zinc was associated with behavioral improvements and reduced DN loss.

For assessing neuronal damage in the substantia nigra, morphometric neuron analysis and immunohistochemical study of the expression level of TH, a marker of DN, were carried out. The topography of the substantia nigra was determined using a stereotactic atlas (Paxinos and Watson 1982). The criterion for determining the location of the lesion (in sham-operated and LPS-lesioned animals) was the presence of a needle track. Morphometric parameters of neurons are shown in Table 1.

The values of intact animals are presented as averages of the right and left anatomical structures. For sham-operated and LPS-lesioned rats, the average values of morphometric parameters of the neurons of the ipsilateral area are presented. Figure 6 shows microphotographs of the injection area (needle track) and the area of damaged substantia nigra. In the group of intact animals, no damaged neurons were found in the study area (Fig. 6A and B). In the group of sham-operated rats, we observed the following lesions: reduction in the number of neurons, glial reaction, and products of cell and erythrocyte destruction (hemosiderin) (Fig. 6C and D).

**Table 1** Morphometric parameters of neurons of the substantia nigra in the rat brain, Me [LQ—UQ]. Notes: *—p<0,05 as compared to intact animals; #—p<0,05 as compared to sham-operated animals; ^—p<0,05 as compared to untreated LPS-lesioned rats (Kruskal–Wallis's test)

| Animal group | Neuronal area, μm$^2$ |
|---|---|
| Intact animals | 500.4 [371.7–701.6] |
| Sham-operated | 283.5 [246.4–343.5]* |
| LPS-PD | 204.0 [158.6–285.3]*# |
| LPS-PD+$^{64}$Zn-asp | 270.6 [215.4–336.4]#^ |

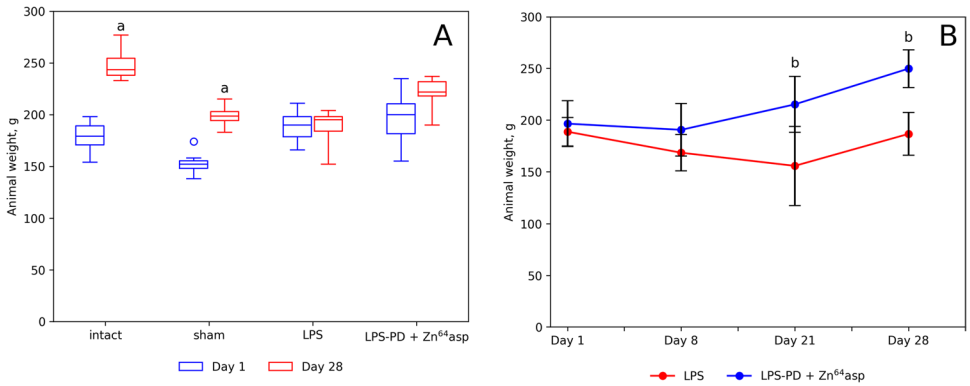


**Fig. 5** Effect of treatment with $^{64}$Zn-asp on body weight in LPS-lesioned rats. A—changes in weight in all groups of animals at the time of experiment cessation; B—weight variation in LPS-lesioned rats with and without treatment with.$^{64}$Zn-asp over the time of the observation. Data are presented as medians and IQR. a – p≤0.05 as compared to the value at Day 1, b—p≤0.05 as compared to untreated LPS-lesioned rats (Mann–Whitney U test)

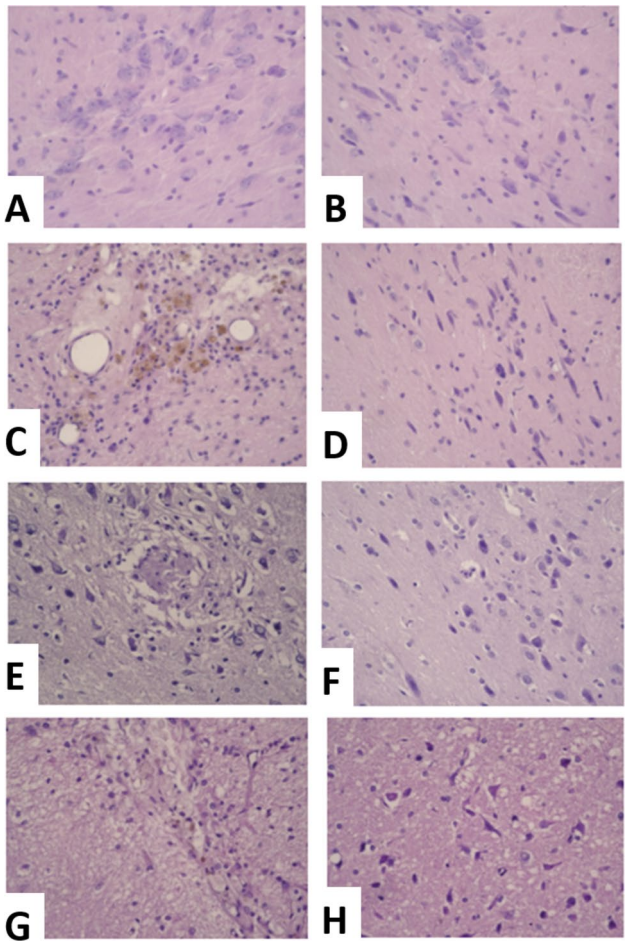


**Fig. 6** Representative photomicrographs of the substantia nigra of the rat brain. H&E staining, magnification × 400. A, B – intact animals; C, D – sham-operated animals; E, F – LPS-PD; G, H – LPS-PD + $Zn^{64}$-asp

The neurons of the substantia nigra were significantly smaller compared to those in intact animals, and dead hyperchromic neurons were detected. The median values of the neuron area in the substantia nigra of sham-operated rats were 283.5 [246.4–343.5] μm2 vs 500.4 [371.7–701.6] μm2 in the intact animals. In the LPS-PD group, the structural changes were similar to those in the sham-operated animals, but much more pronounced (Fig. 6E and F). Edema and gliosis were observed in the area of toxin injection. The neurons in the substantia nigra were deformed, their perikaryon area was significantly smaller, and their number in the microsection projection was reduced as compared to both intact and sham-operated animals. The neuronal area was significantly smaller as compared to the values in the sham-operated group, with a median value of 204.0 [158.6–285.3] μm2 and 283.5 [246.4–343.5] μm2, respectively. In the LPS-lesioned rats that received $^{64}$Zn-asp, the number of neurons with relatively preserved perikaryons was higher than that in untreated animals (Fig. 6G and H), which was reflected in morphometric parameters (a significant increase in neuronal area by 32.6%, $P < 0.05$).

Intrigral LPS injection induced ~ 60% DN degeneration, depicted by reduced immunoreactivity for TH (Fig. 7C). Q values in the LPS-PD group were 3 times lower than those in intact and sham-operated animals. Q values in LPS-lesioned rats treated with $^{64}$Zn-asp (Fig. 7D) were comparable to those in sham-operated rats (Fig. 7A and B). DN loss was also confirmed by the results of apomorphine tests. On Day 8 (7 days after the surgery and day before the treatment initiation), contralateral rotation rate in LPS-injected rats was at an average of 2.2 rpm, indicating ~ 44–60% DN loss (Fig. 8A). On Day 15 (14 days after surgery), 67% of the animals from the LPS-PD group showed a 23% increase in rotation rate, indicating progressive DN loss (Fig. 8A and B), whereas rotation rates of 33% of untreated animals with LPS-PD were unchanged or slightly decreased. In contrast, 86% of the rats from group LPS-PD + $^{64}$Zn-asp demonstrated a 13% decrease in rotation rate, indicating preserving/restoring DN, whereas rotation rates in 14% of the animals from this group were unchanged or slightly increased, indicating progressive DN loss.

We used the open field test and the EPM test for assessing behavioral functions in animals. DN loss in the LPS-lesioned rats was associated with behavioral alterations (Fig. 9). Specifically, spontaneous locomotor activity of the LPS-lesioned rats was reduced as indicated by the

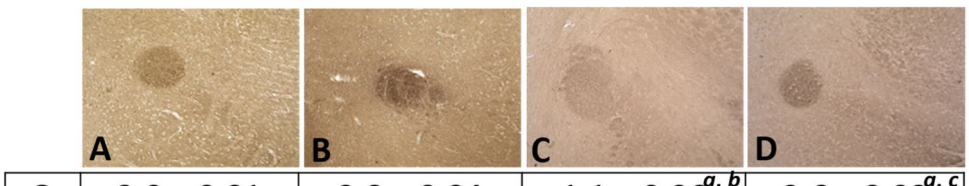


| Q | 3.0 ± 0.01 | 2.8 ± 0.04 | 1.1 ± 0.06$^{a, b}$ | 2.6 ± 0.08$^{a, c}$ |
|---|---|---|---|---|

**Fig. 7** Representative immunohistochemical images of the TH-positive neurons (brown) in hippocampal area: intact animals (A), sham-operated animals (B), LPS-lesioned (C), LPS-PD + $^{64}$Zn-asp, magnification × 50. Quick scores (Q) under the images, calculated by multiplying the percentage of positive cells (P) by the intensity (I) and presented as: Q = P x I, are shown. Data are presented as mean ± SD. a—$p \leq 0.05$ as compared to intact animals, b—$p \leq 0.05$ as compared to sham-operated animals; c—$p \leq 0.05$ as compared to LPS-PD group (ANOVA with Tukey's post-hoc test)

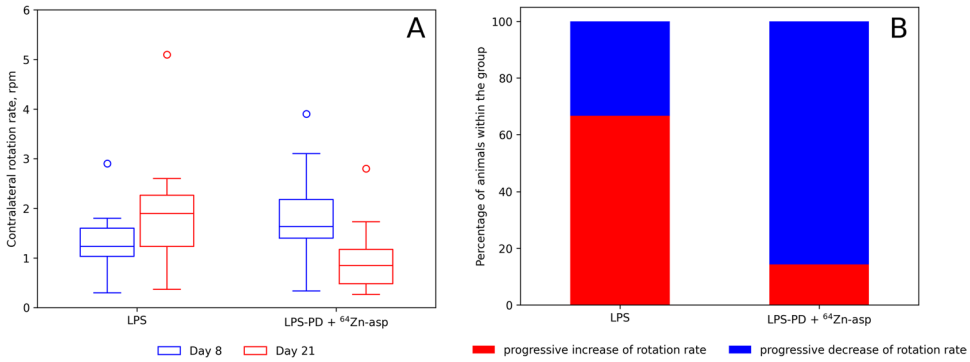


**Fig. 8** Effect of Zn64-asp on apomorphine-induced rotation in LPS-lesioned rats. A – a mean rotation rate in the 1 st and 2nd apomorphine test. Data are presented as medians and IQR. B—percentage of rats with an increase or decrease in rotation rate between the 1 st and 2nd apomorphine test

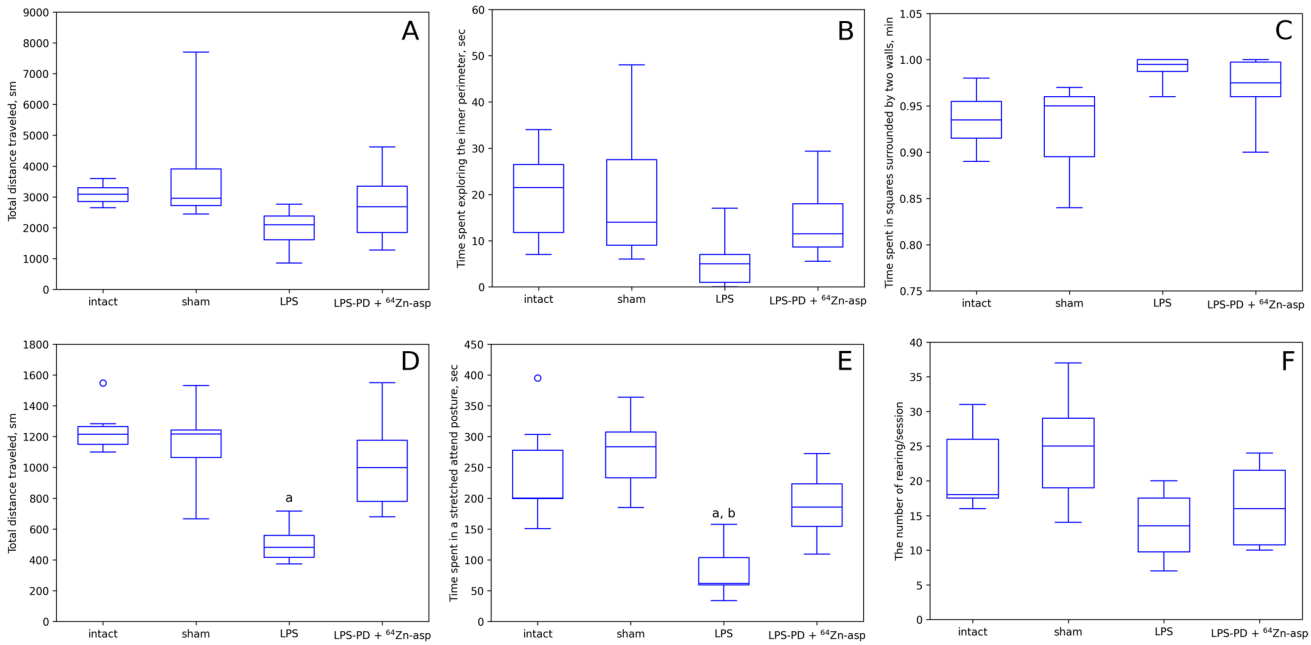


**Fig. 9** Effect of 64Zn-asp on behavioral characteristics of LPS-lesioned rats. A – total distance traveled in open field test; B – time spent exploring the inner perimeter in open field test; C – thigmotaxis behavior in open field test; D—total distance traveled in EMTEPM test; E – risk assessment behavior in EMTEPM test; F – number of rearing in open field test. Data are presented as medians and IQR. a—$p \leq 0.05$ as compared to intact animals, b—$p \leq 0.05$ as compared to sham-operated animals; c—$p \leq 0.05$ as compared to LPS-PD group (Kruskal–Wallis's test)

decreased median value of total distance traveled in open field arena by 37% as compared to control groups ($p = 0.06$) (Fig. 9A), and in EPM-test—by 2.4 times as compared to control groups ($p \leq 0.05$) (Fig. 9D). Treatment with $^{64}$Zn-asp improved LPS-induced locomotor activity impairment – median value of total distance traveled in rats from LPD-PD+$^{64}$Zn-asp group in both tests was higher than that in untreated animals, and did not differ significantly from that in control groups.

By the end of the experiment, LPS-lesioned rats exhibited moderate anxiety-like behavior. The time spent in the inner perimeter of the open field arena by rats in the LPS-PD group was approximately 2.5 times lower than that of the control group ($p > 0.05$) (Fig. 9B). The time spent in squares bordered by two walls, indicative of thigmotaxis, was slightly higher in LPS-lesioned rats compared to the control group (Fig. 9C). The time spent in a stretched attend posture, which reflects risk assessment behavior, was more than twice as low in LPS-lesioned rats compared to control animals (Fig. 9E). In contrast, LPS-lesioned rats treated with $^{64}$Zn-asp exhibited behavior comparable to that of the control group across all these parameters. Rearing frequency was slightly reduced in animals from the LPS-PD group as compared to rats from control groups (Fig. 9F). In animals with LPS-PD treated with $^{64}$Zn-asp, a tendency towards normalizing the rearing was observed. Taken together, these results indicate that the treatment with 64Zn-asp mitigates the anxiogenic effects of LPS.

## Discussion

Over the past two decades, research has highlighted the significant role of neuroinflammation in the degeneration of the nigrostriatal dopaminergic pathway, a key pathological feature of PD. Recognizing the critical role of inflammation in the progression and persistence of PD could open new avenues for therapeutic strategies (Araújo et al. 2022; Grotemeyer et al. 2022). In this study, out of the many PD animal models, we selected a lipopolysaccharide (LPS)-induced one for exploring the anti-inflammatory properties of a novel zinc-based compound. The LPS-induced PD model is commonly used as an inflammatory or immune-related paradigm rather than a comprehensive model of Parkinson's disease. Although it does not reproduce the full spectrum of PD pathology, it recapitulates certain clinically relevant aspects, including motor impairment and some non-motor symptoms (García-Revilla et al. 2022; Deng et al. 2020; Oliynyk et al. 2023). LPS (endotoxin) is a canonical microbe-associated molecular pattern and potent inflammogen, which does not directly affect dopaminergic neurons (Qin et al. 2004). A unilateral injection of LPS into the substantia nigra elicits a robust neuroinflammatory response that can lead to dopaminergic neuron loss (Sanfeliu et al. 2024). Mechanistically, LPS activates the canonical NF-κB pathway (Guo et al. 2024). Interestingly, zinc sulfate has been shown to inhibit LPS-induced inflammatory responses in microglial cells in vitro by interfering with the NF-κB pathway through the up-regulation of A20 expression (Hongxia et al. 2019). Given these considerations, the LPS-induced model, despite its limitations, offers a valuable tool for investigating the effects of a novel zinc preparation on neuroinflammation and related motor dysfunction in lesioned rats.

The form of zinc used in supplements or treatments can significantly impact its bioavailability and therapeutic effects. Over time, zinc supplements have evolved from inorganic to organic forms, largely to address one major limitation of inorganic zinc compounds: low bioavailability (Liu et al. 2023). The isotopically modified zinc employed in this study, $^{64}$Zn-asp, offers an additional benefit, as the chelate complex of $Zn^{2+}$ with aspartic acid has demonstrated allogenic suppressive activity, highlighting its potential for modulating inflammatory immune responses (Piacenza et al. 2023).

Neuroinflammation involves the activation of glial cells in the brain, primarily microglia and astrocytes, which are tightly interconnected. In neurodegenerative diseases, their interaction is initiated by the binding of damage-associated molecular patterns (DAMPs) to Toll-like receptors (TLRs) on the membranes of MG and astrocytes or to intracellular receptors following endocytosis. This process activates downstream signaling pathways (Kam et al. 2020). Both MG and astrocytes can serve as the primary sensors of DAMPs. For example, the activation of TLR4 by α-synuclein in MG stimulates phagocytic activity, the release of pro-inflammatory cytokines, and the production of ROS, which in turn promotes the pro-inflammatory transformation of astrocytes. Additionally, α-synuclein binding to FcγRIIB on MG suppresses their phagocytic function by activating SHP-1, further inhibiting phagocytosis (Zhao et al. 2024). Among activated astrocytes, the pro-inflammatory phenotype intensifies the inflammatory activation of microglia. These astrocytes release a significant number of inflammatory mediators, contributing to excitotoxicity and exacerbating the inflammatory response (Sun et al. 2023). In LPS-lesioned rats in our experiments, reactive astrogliosis with a significant increase of MBP in brain homogenates was registered, indicating demyelination and neuronal damage (Kıray et al. 2016). The anti-inflammatory effect of $^{64}$Zn-asp was evidenced by the reduction of reactive astrogliosis, as was ascertained by a decrease in the level of GFAP and its breakdown products both in brain tissue homogenates and in blood serum, as well as by a significant decrease in MBP in the brain homogenate. Reactive astrogliosis was associated with metabolic changes of MG. LPS is the most potent pro-inflammatory trigger for microglia/macrophages, which transform resting MG of M2 anti-inflammatory homeostatic profile to M1 polarized reactive cells (Allendorf et al. 2020). However, the functional state of the complex population of microglia/macrophages in neuroinflammation does not fit within the simplified M1/M2 paradigm. First, inflamed MG contains cells with different profiles: M1 (classical activation), M2 (alternative activation or 'acquired deactivation'), including intermediate phenotypes M2a, M2b, M2c. Second, as mentioned above, the brain-resident phagocyte population contains MG and BAM. In adults, MG and BAM possess distinct functions in the brain. MGs are self-renewed, highly phagocytic, and are mostly responsible for tissue homeostasis maintenance by scavenging cell debris and synapses, mediating neurogenesis in central nervous system injury, etc. BAM are answerable for the immune surveillance of pathological antigens and are endowed with increased antigen-presenting capacity with CD86 overexpression. The principal phenotypic marker differentiating MG and BAM is CD206. Resting MG is CD206-, reactive MG is CD206low. BAM are CD206high (Wen et al. 2024; Sun & Jiang 2024). Single stereotaxic LPS injection was reported to increase accumulating cytoplasmic α-synuclein in nigral TH-positive neurons (Choi et al. 2009; Deng et al. 2020). CD206- MG is vital in scavenging α-synuclein. However, excessive α-synuclein production could overwhelm its scavenging and, consequently, can increase extracellular α-synuclein protein. As stated above,

extracellular α-synuclein acts as a DAMP for MG, inducing the NFκB signaling pathway through TLR, and transforming resting cells into reactive cells, which is accompanied by blocking MG phagocytic activity and a decrease in α-synuclein clearing (Miao and Meng 2024). In our experiments, treatment of LPS-lesioned rats with $^{64}$Zn-asp was accompanied by a significant increase in microglia/macrophage phagocytic activity, in such a way restoring homeostatic scavenging capacity of these cells, which in turn could facilitate the resolution of neuroinflammation. In addition, treatment with 64Zn-asp was associated with a decrease in CD86 + and CD206 + cell count. Given that the BAM subset mostly represents CD86 + and CD206 + cell fractions in the complex microglia/macrophage population and may be replenished by the circulating monocytes during inflammation, this effect may be explained by the inhibitory effect of $^{64}$Zn-asp on inflammatory blood cell recruitment.

Reduced neuroinflammation in rats with LPS-PD that received the i.v. $^{64}$Zn-asp treatment was correlated with moderately reduced manifestation of motor and non-motor symptoms of the disease. The treatment course of i.v. $^{64}$Zn-asp injections mitigated weight loss, alleviated anxiety-like behavior, and reduced locomotor activity impairment. Weight loss in animal PD models is partly related to anxiety-like behavior, which (along with impairment of locomotor activity) is in turn associated with loss of dopaminergic and serotonergic neurons. The improvement in motor and non-motor symptoms observed in LPS-lesioned rats treated with $^{64}$Zn-asp can likely be attributed to the prevention of dopaminergic neuron (DN) loss and/or their restoration. This conclusion is supported by the findings from the histological analysis, the apomorphine test, and immunostaining for tyrosine hydroxylase (TH). Increased blood–brain barrier permeability, caused by LPS-induced inflammation (Jangula and Murphy 2013), allowed zinc movement to the brain tissues. The reduction in DN loss in the $^{64}$Zn-asp-treated animals may be the result of the anti-inflammatory effect of $^{64}$Zn-asp aimed at restraining the pro-inflammatory and neuroprotective profile of microglia/macrophages and astroglia involved in neuroinflammation. On the other hand, considering that zinc regulates cell proliferation (Fan et al. 2024), attenuated DN loss in treated animals could be attributed to the stimulated proliferation and differentiation of neural stem cells.

In conclusion, neuroinflammation is a critical driver of PD pathogenesis, underscoring the importance of anti-inflammatory therapeutic strategies. In this study, the LPS-induced PD model exhibited reactive astrogliosis and a pro-inflammatory metabolic shift in MG/BAM cells, both of which were attenuated by intravenous $^{64}$Zn-asp, leading to improvements in cognitive performance.

Several limitations should be acknowledged. The considerable variability in behavioral and biochemical outcomes highlights the need for larger cohorts to strengthen statistical power. In addition, the effects of $^{64}$Zn-asp on zinc homeostasis and direct neuronal function were not examined, leaving aspects of its mechanism unresolved. Finally, although the LPS model offers a valuable platform to study neuroinflammation and reproduces selected motor and non-motor features of PD, it remains primarily an immune-related paradigm and does not capture the full complexity of the disease.

Taken together, these findings suggest that $^{64}$Zn-asp holds promise as a therapeutic strategy to mitigate neuroinflammation and cognitive impairment in PD, while also highlighting the need for validation in complementary models and translational settings.

**Supplementary Information** The online version contains supplementary material available at https://doi.org/10.1007/s11481-025-10257-8.

**Acknowledgements** Not applicable

**Author Contribution** M.T.: supervision and writing—review and editing. M.R.: methodology, investigation, formal analysis. A.B.: methodology, conceptualization, and project administration. S.G.: conceptualization, writing—review and editing. T.D.: methodology, investigation. R.B.: methodology, conceptualization. N.D.: methodology, investigation. G.T.: supervision and writing—review and editing. L.S.: methodology, conceptualization, project administration and writing—original draft. All authors reviewed the final version of the manuscript.

**Funding** The study was supported by a TSNUK project N 18DP36-10.

**Data Availability** The data that support the findings of this study are available from the corresponding author, upon reasonable request.

## Declarations

**Competing interests** The authors declare no competing interests.

**Open Access** This article is licensed under a Creative Commons Attribution-NonCommercial-NoDerivatives 4.0 International License, which permits any non-commercial use, sharing, distribution and reproduction in any medium or format, as long as you give appropriate credit to the original author(s) and the source, provide a link to the Creative Commons licence, and indicate if you modified the licensed material. You do not have permission under this licence to share adapted material derived from this article or parts of it. The images or other third party material in this article are included in the article's Creative Commons licence, unless indicated otherwise in a credit line to the material. If material is not included in the article's Creative Commons licence and your intended use is not permitted by statutory regulation or exceeds the permitted use, you will need to obtain permission directly from the copyright holder. To view a copy of this licence, visit http://creativecommons.org/licenses/by-nc-nd/4.0/.

## References


Adam H, Gopinath SCB, Md Arshad MK, Adam T, Parmin NA, Husein I, Hashim U (2023) An update on pathogenesis and clinical scenario for Parkinson's disease: diagnosis and treatment. 3 Biotech 13(5):142. https://doi.org/10.1007/s13205-023-03553-8

Alam A, Hana Z, Jin Z, Suen KC, Ma D (2018) Surgery, neuroinflammation and cognitive impairment. EBioMedicine 37:547–556. https://doi.org/10.1016/j.ebiom.2018.10.021

Albarede F, Télouk P, Balter V, Bondanese VP, Albalat E, Oger P, Bonaventura P, Miossec P, Fujii T (2016) Medical applications of Cu, Zn, and S isotope effects. Metallomics 8(10):1056–1070. https://doi.org/10.1039/c5mt00316d

Alfaidi M, Barker RA, Kuan WL (2024) An update on immune-based alpha-synuclein trials in Parkinson's disease. J Neurol 272(1):21. https://doi.org/10.1007/s00415-024-12770-x

Al-Harthi S, Kharchenko V, Mandal P, Gourdoupis S, Jaremko Ł (2022) Zinc ions prevent α-synuclein aggregation by enhancing chaperone function of human serum albumin. Int J Biol Macromol 222(Pt B):2878–2887. https://doi.org/10.1016/j.ijbiomac.2022.10.066

Allendorf DH, Franssen EH, Brown GC (2020) Lipopolysaccharide activates microglia via neuraminidase 1 desialylation of Toll-like receptor 4. J Neurochem 155(4):403–416. https://doi.org/10.1111/jnc.15024

Araújo B, Caridade-Silva R, Soares-Guedes C, Martins-Macedo J, Gomes ED, Monteiro S, Teixeira FG (2022) Neuroinflammation and Parkinson's disease-from neurodegeneration to therapeutic opportunities. Cells 11(18):2908. https://doi.org/10.3390/cells11182908

Baarz BR, Laurentius T, Wolf J, Wessels I, Bollheimer LC, Rink L (2022) Short-term zinc supplementation of zinc-deficient seniors counteracts CREMα - mediated IL-2 suppression. Immun Ageing 19(1):40. https://doi.org/10.1186/s12979-022-00295-8

Baltaci SB, Gümüş H, Ünal Ö, Acar G, Bayiroğlu AF (2024) Zinc supplementation improves ZIP14 (SLC39A14) levels in cerebral cortex suppressed by icv-STZ injection. Noro Psikiyatr Ars 61(1):11–14. https://doi.org/10.29399/npa.28426

Berg D, Eggert K, Haslinger B, Kassubek J, Mollenhauer B, Reetz K, Rogge A, Schaeffer E, Tönges L, Zeuner KE (2020) Disease modifying treatment trials in Parkinson's disease: how to balance expectations and interests of patients, physicians and industry partners? Neurol Res Pract 2:31. https://doi.org/10.1186/s42466-020-00076-y

Brown DR (2009) Metal binding to alpha-synuclein peptides and its contribution to toxicity. Biochem Biophys Res Commun 380(2):377–381. https://doi.org/10.1016/j.bbrc.2009.01.103

Buesa RJ, Peshkov MV (2011) Complete elimination of xylene in practice of a histology laboratory. Arkh Patol 73:54–60

Chan Y, Walmsley RP (1997) Learning and understanding the Kruskal-Wallis one-way analysis-of-variance-by-ranks test for differences among three or more independent groups. Phys Ther 77(12):1755–1762. https://doi.org/10.1093/ptj/77.12.1755

Chen C, Turnbull DM, Reeve AK (2019) Mitochondrial dysfunction in Parkinson's disease-cause or consequence? Biology 8(2):38. https://doi.org/10.3390/biology8020038

Choi DY, Liu M, Hunter RL, Cass WA, Pandya JD, Sullivan PG, Shin EJ, Kim HC, Gash DM, Bing G (2009) Striatal neuroinflammation promotes Parkinsonism in rats. PLoS ONE 4(5):e5482. https://doi.org/10.1371/journal.pone.0005482

Çınar E, Tel BC, Şahin G (2022) Neuroinflammation in Parkinson's disease and its treatment opportunities. Balkan Med J 39(5):318–333. https://doi.org/10.4274/balkanmedj.galenos.2022.2022-7-100

Cornice J, Verzella D, Arboretto P, Vecchiotti D, Capece D, Zazzeroni F, Franzoso G (2024) NF-κB: governing macrophages in cancer. Genes 15(2):197. https://doi.org/10.3390/genes15020197

Cumming K, Macleod AD, Myint PK, Counsell CE (2017) Early weight loss in parkinsonism predicts poor outcomes: evidence from an incident cohort study. Neurology 89(22):2254–2261. https://doi.org/10.1212/WNL.0000000000004691

Cvijanovich NZ, King JC, Flori HR, Gildengorin G, Vinks AA, Wong HR (2016) Safety and dose escalation study of intravenous zinc supplementation in pediatric critical illness. J Parenter Enteral Nutr 40(6):860–868. https://doi.org/10.1177/0148607115572193

Dabravolski SA, Sadykhov NK, Kartuesov AG, Borisov EE, Sukhorukov VN, Orekhov AN (2022) Interplay between Zn2+ homeostasis and mitochondrial functions in cardiovascular diseases and heart ageing. Int J Mol Sci 23(13):6890. https://doi.org/10.3390/ijms23136890

de Oliveira NL, Tavares VDO, Agrícola PMD, de Oliveira LP, Sales MC, de Sena-Evangelista KCM, Gomes IC, Galvão-Coelho NL, Pedrosa LFC, Lima KC (2021) Factors associated with inflammaging in institutionalized older people. Sci Rep 11(1):18333. https://doi.org/10.1038/s41598-021-97225-3

Deng I, Corrigan F, Zhai G, Zhou XF, Bobrovskaya L (2020) Lipopolysaccharide animal models of Parkinson's disease: recent progress and relevance to clinical disease. Brain Behav Immun 4:100060. https://doi.org/10.1016/j.bbih.2020.100060

Falkeholm L, Grant CA, Magnusson A, Mollur E (2001) Xylene-free method for histological preparation: A Multicentre Evaluation. Lab Invest 81(9):1213–1221. https://doi.org/10.1038/labinvest.3780335

Fan YG, Wu TY, Zhao LX, Jia RJ, Ren H, Hou WJ, Wang ZY (2024) From zinc homeostasis to disease progression: unveiling the neurodegenerative puzzle. Pharmacol Res 199:107039. https://doi.org/10.1016/j.phrs.2023.107039

Ferreira AFF, Binda KH, Singulani MP, Pereira CPM, Ferrari GD, Alberici LC, Real CC, Britto LR (2020) Physical exercise protects against mitochondria alterations in the 6-hidroxydopamine rat model of Parkinson's disease. Behav Brain Res 387:112607. https://doi.org/10.1016/j.bbr.2020.112607

Forloni G, La Vitola P, Cerovic M, Balducci C (2021) Inflammation and Parkinson's disease pathogenesis: mechanisms and therapeutic insight. Prog Mol Biol Transl Sci 177:175–202. https://doi.org/10.1016/bs.pmbts.2020.11.001

Frank MG, Wieseler-Frank JL, Watkins LR, Maier SF (2006) Rapid isolation of highly enriched and quiescent microglia from adult rat hippocampus: immunophenotypic and functional characteristics. J Neurosci Methods 151(2):121–130. https://doi.org/10.1016/j.jneumeth.2005.06.026

Gage GJ, Kipke DR, Shain W (2012) Whole animal perfusion fixation for rodents. J vis Exp 30:65. https://doi.org/10.3791/3564

Gammoh NZ, Rink L (2017) Zinc in infection and inflammation. Nutrients 9(6):624. https://doi.org/10.3390/nu9060624

García-Revilla J, Herrera AJ, de Pablos RM, Venero JL (2022) Inflammatory animal models of Parkinson's disease. J Parkinsons Dis 12(s1):S165–S182. https://doi.org/10.3233/JPD-213138

Grotemeyer A, McFleder RL, Wu J, Wischhusen J, Ip CW (2022) Neuroinflammation in Parkinson's disease - putative pathomechanisms and targets for disease-modification. Front Immunol 13:878771. https://doi.org/10.3389/fimmu.2022.878771

Gumus H, Baltaci SB, Unal O, Gulbahce-Mutlu E, Mogulkoc R, Baltaci AK (2023) Zinc ameliorates Nogo-A receptor and osteocalcin gene expression in memory-sensitive rat hippocampus impaired by intracerebroventricular injection of streptozotocin. Biol Trace Elem Res 201(7):3381–3386. https://doi.org/10.1007/s12011-022-03410-4

Guo Q, Jin Y, Chen X, Ye X, Shen X, Lin M, Zeng C, Zhou T, Zhang J (2024) NF-κB in biology and targeted therapy: new insights and

translational implications. Signal Transduct Target Ther 9(1):53. https://doi.org/10.1038/s41392-024-01757-9

Hoban DB, Connaughton E, Connaughton C, Hogan G, Thornton C, Mulcahy P, Moloney TC, Dowd E (2013) Further characterisation of the LPS model of Parkinson's disease: a comparison of intra-nigral and intra-striatal lipopolysaccharide administration on motor function, microgliosis and nigrostriatal neurodegeneration in the rat. Brain Behav Immun 27(1):91–100. https://doi.org/10.1016/j.bbi.2012.10.001

Hommel ALAJ, Krijthe JH, Darweesh S, Bloem BR (2022) The association of comorbidity with Parkinson's disease-related hospitalizations. Parkinsonism Relat Disord 104:123–128. https://doi.org/10.1016/j.parkreldis.2022.10.012

Hongxia L, Yuxiao T, Zhilei S, Yan S, Yicui Q, Jiamin S, Xin X, Jianxin Y, Fengfeng M, Hui S (2019) Zinc inhibited LPS-induced inflammatory responses by upregulating A20 expression in microglia BV2 cells. J Affect Disord 249:136–142. https://doi.org/10.1016/j.jad.2019.02.041

Jangula A, Murphy EJ (2013) Lipopolysaccharide-induced blood brain barrier permeability is enhanced by alpha-synuclein expression. Neurosci Lett 551:23–27. https://doi.org/10.1016/j.neulet.2013.06.058

Jaouen K, Pouilloux L, Balter V, Pons ML, Hublin JJ, Albarède F (2019) Dynamic homeostasis modeling of Zn isotope ratios in the human body. Metallomics 11(6):1049–1059. https://doi.org/10.1039/c8mt00286j

Kam TI, Hinkle JT, Dawson TM, Dawson VL (2020) Microglia and astrocyte dysfunction in Parkinson's disease. Neurobiol Dis 144:105028. https://doi.org/10.1016/j.nbd.2020.105028

Khrieba MO, Hegazy SK, Mustafa W, El-Haggar SM (2024) Repurposing celecoxib as adjuvant therapy in patients with Parkinsonian disease: a new therapeutic dawn: randomized controlled pilot study. Inflammopharmacology 32(6):3729–3738. https://doi.org/10.1007/s10787-024-01567-z

Kıray H, Lindsay SL, Hosseinzadeh S, Barnett SC (2016) The multifaceted role of astrocytes in regulating myelination. Exp Neurol 283(Pt B):541–549. https://doi.org/10.1016/j.expneurol.2016.03.009

Kisucká A, Bimbová K, Bačová M, Gálik J, Lukáčová N (2021) Activation of neuroprotective microglia and astrocytes at the lesion site and in the adjacent segments is crucial for spontaneous locomotor recovery after spinal cord injury. Cells 10(8):1943. https://doi.org/10.3390/cells10081943

Kwon HS, Koh SH (2020) Neuroinflammation in neurodegenerative disorders: the roles of microglia and astrocytes. Transl Neurodegener 9(1):42. https://doi.org/10.1186/s40035-020-00221-2

Lamprea MR, Cardenas FP, Setem J, Morato S (2008) Thigmotactic responses in an open-field. Braz J Med Biol Res 41(2):135–140. https://doi.org/10.1590/s0100-879x2008000200010

Lee Y, Lee S, Chang SC, Lee J (2019) Significant roles of neuroinflammation in Parkinson's disease: therapeutic targets for PD prevention. Arch Pharm Res 42(5):416–425. https://doi.org/10.1007/s12272-019-01133-0

Leite-Almeida H, Almeida-Torres L, Mesquita AR, Pertovaara A, Sousa N, Cerqueira JJ, Almeida A (2009) The impact of age on emotional and cognitive behaviours triggered by experimental neuropathy in rats. Pain 144(1–2):57–65. https://doi.org/10.1016/j.pain.2009.02.024

Liddelow SA, Guttenplan KA, Clarke LE, Bennett FC, Bohlen CJ, Schirmer L, Bennett ML, Münch AE, Chung WS, Peterson TC, Wilton DK, Frouin A, Napier BA, Panicker N, Kumar M, Buckwalter MS, Rowitch DH, Dawson VL, Dawson TM, Stevens B, Barres BA (2017) Neurotoxic reactive astrocytes are induced by activated microglia. Nature 541(7638):481–487. https://doi.org/10.1038/nature21029

Liu S, Wang N, Long Y, Wu Z, Zhou S (2023) Zinc homeostasis: an emerging therapeutic target for neuroinflammation related diseases. Biomolecules 13(3):416. https://doi.org/10.3390/biom13030416

Mbiydzenyuy NE, Ninsiima HI, Valladares MB, Pieme CA (2018) Zinc and linoleic acid pre-treatment attenuates biochemical and histological changes in the midbrain of rats with rotenone-induced Parkinsonism. BMC Neurosci 19(1):29. https://doi.org/10.1186/s12868-018-0429-9

Miao Y, Meng H (2024) The involvement of α-synucleinopathy in the disruption of microglial homeostasis contributes to the pathogenesis of Parkinson's disease. Cell Commun Signal 22(1):31. https://doi.org/10.1186/s12964-023-01402-y

Mishra P, Pandey CM, Singh U, Gupta A, Sahu C, Keshri A (2019) Descriptive statistics and normality tests for statistical data. Ann Card Anaesth 22(1):67–72. https://doi.org/10.4103/aca.ACA_157_18

Mousaviyan R, Davoodian N, Alizadeh F, Ghasemi-Kasman M, Mousavi SA, Shaerzadeh F, Kazemi H (2021) Zinc supplementation during pregnancy alleviates lipopolysaccharide-induced glial activation and inflammatory markers expression in a rat model of maternal immune activation. Biol Trace Elem Res 199(11):4193–4204. https://doi.org/10.1007/s12011-020-02553-6

Moynier F, Borgne ML, Lahoud E, Mahan B, Mouton-Liger F, Hugon J, Paquet C (2020) Copper and zinc isotopic excursions in the human brain affected by Alzheimer's disease. Alzheimers Dement (Amst) 12(1):e12112. https://doi.org/10.1002/dad2.12112

Mussbacher M, Derler M, Basílio J, Schmid JA (2023) NF-κB in monocytes and macrophages - an inflammatory master regulator in multitalented immune cells. Front Immunol 14:1134661. https://doi.org/10.3389/fimmu.2023.1134661

Nakamura R, Tomizawa I, Iwai A, Ikeda T, Hirayama K, Chiu YW, Suzuki T, Tarutani A, Mano T, Iwata A, Toda T, Sohma Y, Kanai M, Hori Y, Tomita T (2023) Photo-oxygenation of histidine residue inhibits α-synuclein aggregation. FASEB J 37(12):e23311. https://doi.org/10.1096/fj.202301533R

Nash B, Ioannidou K, Barnett SC (2011) Astrocyte phenotypes and their relationship to myelination. J Anat Jul 219(1):44–52. https://doi.org/10.1111/j.1469-7580.2010.01330.x

Novak P, Balakin A, Temnik M (2022a) In vitro anticancer activity of the light stable zinc isotope (64Zn) compounds. Anticancer Res 42(12):5685–5698. https://doi.org/10.21873/anticanres.16077

Novak P, Temnikov M, Balakin O (2022b) Pharmaceutical composition for improving health, cure abnormalities and degenerative disease, achieve anti-aging effect of therapy and therapeutic effect on mammals and method thereof. Pharm Compos Improv Health, Cure. Retrieved May 23, 2025, from https://patents.google.com/patent/US20200000845A1/en

Oliynyk Z, Rudyk M, Dovbynchuk T, Dzubenko N, Tolstanova G, Skivka L (2023) Inflammatory hallmarks in 6-OHDA- and LPS-induced Parkinson's disease in rats. Brain Behav Immun 30:100616. https://doi.org/10.1016/j.bbih.2023.100616

Park JS, Koentjoro B, Veivers D, Mackay-Sim A, Sue CM (2014) Parkinson's disease-associated human ATP13A2 (PARK9) deficiency causes zinc dyshomeostasis and mitochondrial dysfunction. Hum Mol Genet 23(11):2802–2815. https://doi.org/10.1093/hmg/ddt623

Pauletti G, Dandekar S, Rong H, Ramos L, Peng H, Seshadri R, Slamon DJ (2000) Assessment of methods for tissue-based detection of the HER-2/neu alteration in human breast cancer: a direct comparison of fluorescence in situ hybridization and immunohistochemistry. J Clin Oncol 18(21):3651–6364. https://doi.org/10.1200/JCO.2000.18.21.3651

Paxinos G, Watson C (1982) The rat brain in stereotaxic coordinats. Academic Press

Pérez S, Rius-Pérez S (2022) Macrophage polarization and reprogramming in acute inflammation: a redox perspective. Antioxidants 11(7):1394. https://doi.org/10.3390/antiox11071394

Piacenza F, Giacconi R, Costarelli L, Malavolta M (2023) Preliminary comparison of fractional absorption of zinc sulphate, zinc gluconate, and zinc aspartate after oral supplementation in healthy human volunteers. Nutrients 15(8):1885. https://doi.org/10.3390/nu15081885

Qin L, Liu Y, Wang T, Wei SJ, Block ML, Wilson B, Liu B, Hong JS (2004) NADPH oxidase mediates lipopolysaccharide-induced neurotoxicity and proinflammatory gene expression in activated microglia. J Biol Chem 279(2):1415–1421. https://doi.org/10.1074/jbc.M307657200

Ramis R, Ortega-Castro J, Vilanova B, Adrover M, Frau J (2018) A systematic DFT study of some plausible Zn(II) and Al(III) interaction sites in N-terminally acetylated α-synuclein. J Phys Chem A 122(2):690–699. https://doi.org/10.1021/acs.jpca.7b10744

Reddy SS, Addi UR, Pullakhandam R, Reddy GB (2022) Dietary zinc deficiency disrupts skeletal muscle proteostasis and mitochondrial biology in rats. Nutrition 98:111625. https://doi.org/10.1016/j.nut.2022.111625

Rudyk MP, Pozur VV, Voieikova DO, Hurmach YV, Khranovska NM, Skachkova OV, Svyatetska VM, Fedorchuk OG, Skivka LM, Berehova TV, Ostapchenko LI (2018) Sex-based differences in phagocyte metabolic profile in rats with monosodium glutamate-induced obesity. Sci Rep 8(1):5419. https://doi.org/10.1038/s41598-018-23664-0

Safiri S, Noori M, Nejadghaderi SA, Mousavi SE, Sullman MJM, Araj-Khodaei M, Singh K, Kolahi AA, Gharagozli K (2023) The burden of Parkinson's disease in the Middle East and North Africa region, 1990–2019: results from the global burden of disease study 2019. BMC Public Health 23(1):107. https://doi.org/10.1186/s12889-023-15018-x

Saini N, Schaffner W (2010) Zinc supplement greatly improves the condition of parkin mutant Drosophila. Biol Chem 391(5):513–518. https://doi.org/10.1515/BC.2010.052

Sameei P, Fatehfar S, Abdollahzadeh N, Chodari L, Saboory E, Roshan-Milani S (2023) The effects of forced exercise and zinc supplementation during pregnancy on prenatally stress-induced behavioral and neurobiological consequences in adolescent female rat offspring. Dev Psychobiol 65(6):e22411. https://doi.org/10.1002/dev.22411

Sanfeliu C, Bartra C, Suñol C, Rodríguez-Farré E (2024) New insights in animal models of neurotoxicity-induced neurodegeneration. Front Neurosci 17:1248727. https://doi.org/10.3389/fnins.2023.1248727

Sestakova N, Puzserova A, Kluknavsky M, Bernatova I (2013) Determination of motor activity and anxiety-related behaviour in rodents: methodological aspects and role of nitric oxide. Interdiscip Toxicol 6(3):126–135. https://doi.org/10.2478/intox-2013-0020

Silvin A, Qian J, Ginhoux F (2023) Brain macrophage development, diversity and dysregulation in health and disease. Cell Mol Immunol 20(11):1277–1289. https://doi.org/10.1038/s41423-023-01053-6

Solovyev N, El-Khatib AH, Costas-Rodríguez M, Schwab K, Griffin E, Raab A, Platt B, Theuring F, Vogl J, Vanhaecke F (2021) Cu, Fe, and Zn isotope ratios in murine Alzheimer's disease models suggest specific signatures of amyloidogenesis and tauopathy. J Biol Chem 296:100292. https://doi.org/10.1016/j.jbc.2021.100292

Song J, Zhao Y, Shan X, Luo Y, Hao N, Zhao L (2024) Active ingredients of Chinese medicine with immunomodulatory properties: NF-κB pathway and Parkinson's disease. Brain Res 1822:148603. https://doi.org/10.1016/j.brainres.2023.148603

Sun M, You H, Hu X, Luo Y, Zhang Z, Song Y, An J, Lu H (2023) Microglia-astrocyte interaction in neural development and neural pathogenesis. Cells 12(15):1942. https://doi.org/10.3390/cells12151942

Sun R, Jiang H (2024) Border-associated macrophages in the central nervous system. Clin Immunol 109921. https://doi.org/10.1016/j.clim.2024.109921

Talanov SA, Oleshko NN, Tkachenko MN, Sagach VF (2006) Pharmacoprotective influences on different links of the mechanism underlying 6-hydroxydopamineinduced degeneration of nigrostriatal dopaminergic neurons. Neurophysiology 38(2):128–133. https://doi.org/10.1007/s11062-006-0035-9

Tanaka YK, Hirata T (2018) Stable isotope composition of metal elements in biological samples as tracers for element metabolism. Anal Sci 34(6):645–655. https://doi.org/10.2116/analsci.18SBR02

Walf AA, Frye CA (2007) The use of the elevated plus maze as an assay of anxiety-related behavior in rodents. Nat Protoc 2(2):322–328. https://doi.org/10.1038/nprot.2007.44

Walsh S, Finn DP, Dowd E (2011) Time-course of nigrostriatal neurodegeneration and neuroinflammation in the 6-hydroxydopamine-induced axonal and terminal lesion models of Parkinson's disease in the rat. Neuroscience 175:251–261. https://doi.org/10.1016/j.neuroscience.2010.12.005

Wang J, He W, Zhang J (2023) A richer and more diverse future for microglia phenotypes. Heliyon 9(4):e14713. https://doi.org/10.1016/j.heliyon.2023.e14713

Weil MT, Möbius W, Winkler A, Ruhwedel T, Wrzos C, Romanelli E, Bennett JL, Enz L, Goebels N, Nave KA, Kerschensteiner M, Schaeren-Wiemers N, Stadelmann C, Simons M (2016) Loss of myelin basic protein function triggers myelin breakdown in models of demyelinating diseases. Cell Rep 16(2):314–322. https://doi.org/10.1016/j.celrep.2016.06.008

Wen W, Cheng J, Tang Y (2024) Brain perivascular macrophages: current understanding and future prospects. Brain 147(1):39–55. https://doi.org/10.1093/brain/awad304

Wessels I, Maywald M, Rink L (2017) Zinc as a gatekeeper of immune function. Nutrients 9(12):1286. https://doi.org/10.3390/nu9121286

Willis AW, Roberts E, Beck JC, Fiske B, Ross W, Savica R, Van Den Eeden SK, Tanner CM, Marras C, Parkinson's Foundation P4 Group (2022) Incidence of Parkinson disease in North America. NPJ Parkinsons Dis 8(1):170. https://doi.org/10.1038/s41531-022-00410-y

Yamashita KY, Bhoopatiraju S, Silverglate BD, Grossberg GT (2023) Biomarkers in Parkinson's disease: a state of the art review. Biomark Neuropsy 9:100074. https://doi.org/10.1016/j.bionps.2023.100074

Yunna C, Mengru H, Lei W, Weidong C (2020) Macrophage M1/M2 polarization. Eur J Pharmacol 877:173090. https://doi.org/10.1016/j.ejphar.2020.173090

Zhao Y, Huang Y, Cao Y, Yang J (2024) Astrocyte-mediated neuroinflammation in neurological conditions. Biomolecules 14(10):1204. https://doi.org/10.3390/biom14101204

Zhu F, Yue W, Wang Y (2014) The nuclear factor kappa B (NF-κB) activation is required for phagocytosis of *staphylococcus aureus* by RAW 264.7 cells. Exp Cell Res 327(2):256–263. https://doi.org/10.1016/j.yexcr.2014.04.018

**Publisher's Note** Springer Nature remains neutral with regard to jurisdictional claims in published maps and institutional affiliations.